Supplementary Information (SI) for Chemical Science.

Supporting Information

Ultra-Wide Time-Dependent Phosphorescence Color of Carbon Dots via Synergistic Strategy of Dual Confinement Structures Constructing Multiple Luminescent Centers

Shiwei Zhang[a#], Chenglong Shen[b#], Jiurong Li[a], Junfei Liao[a], Peng Miao*[c], Xiujian Zhao[a], and Xiao Gong*[a]

a. State Key Laboratory of Silicate Materials for Architectures, Wuhan University of Technology, Wuhan 430070, P. R. China.

b. Henan Key Laboratory of Diamond Optoelectronic Materials and Devices, Key Laboratory of Material Physics, Ministry of Education, and School of Physics and Microelectronics, Zhengzhou University, Zhengzhou 450052, China

c. Suzhou Institute of Biomedical Engineering and Technology, Chinese Academy of Sciences, Suzhou 215163, P. R. China

* Corresponding author:

E-mail address: miaopeng@sibet.ac.cn (P. Miao); xgong@whut.edu.cn (X. Gong)

\# equal contribution

Experimental Section

Materials

1,4,5,8-Naphthalenetetracarboxylic acid (containing Monoanhydride) (1,4,5,8-NTA), 3-aminopropyltriethoxysilane (APTES), and urea were purchased from Aladdin Chemical Co. Boric acid (BA) were purchased from China National Pharmaceutical Group Chemical Reagent Co. Deionized water (DI water) was made from the laboratory.

Synthesis of Si-NTA/NTA

Si-NTA was synthesized by a simple hydrothermal method. Briefly, 0.1 g of 1,4,5,8-NTA and 0.5 mL of APTES were dissolved in 10 mL DI water solution, and the solution was transferred into a poly(tetrafluoroethylene) (Teflon)-lined autoclave (20 mL) and heated at 180 °C for 2 h to obtain a pale green solution. After being cooled, the solution was then centrifuged at 8000 rpm for 3 min to remove the precipitate. The purified Si-NTA solution was filtered through a polycarbonate membrane filter (from Filter-Lab) with a pore size of 0.22 μm to remove impurities. Similarly, the NTA were prepared using only 1,4,5,8-NTA for the hydrothermal reaction. The remainder of post-treatment conditions were identical to those used for the Si-NTA solution.

Synthesis of Si-CDs@B_2O_3

In this work, 0.5 mL of Si-NTA solution, DI water (10 mL), and BA (2 g) were added to a crucible and stirred for 5 min at room temperature to homogenize the Si-NTA and BA, and then transferred to an oven at 200 °C and heated continuously for 4 h to get Si- CDs@B_2O_3. After cooling, the material was ground to obtain Si-CDs@B_2O_3 powder.

Synthesis of Si-CDs@Urea/CDs@B_2O_3/CDs@Urea

The synthesis of Si-CDs@Urea, CDs@B_2O_3, and CDs@Urea is analogous to that of Si-CDs@B_2O_3. In the synthesis of Si-CDs@Urea, BA was replaced with urea (2 g).

Similarly, the synthesis of CDs@B_2O_3 entails the replacement of Si-NTA with NTA (0.5 mL), and the substitution of Si-NTA and BA with NTA (0.5 mL) and urea (2 g), respectively, to yield CDs@Urea.

Synthesis of N@SiO_2@B_2O_3/N@B_2O_3/N@Urea/N@SiO_2

In a crucible, 1,4,5,8-NTA (0.02 g), APTES (0.2 mL), and 10 mL of DI water were combined and stirred for 5 min to achieve homogeneity. The mixture was then transferred to an oven and heated at 200 °C for 4 h. After cooling, the material was ground to obtain N@SiO_2@B_2O_3 powder. Similarly, precursors were replaced with 1,4,5,8-NTA (0.02 g) and BA (2 g), 1,4,5,8-NTA (0.02 g) and urea (2 g), and 1,4,5,8-NTA (0.02 g) and APTES (0.2 mL) to obtain N@B_2O_3, N@Urea, and N@SiO_2 powders, respectively.

Characterization

Nuclear magnetic resonance (NMR) spectra were measured using NMR spectrometer (Bruker AVANCEIII 400M), and High-resolution mass spectrometry (HR-MS) were recorded using a Bruker solan X 70 FT-MS. TEM and HR-TEM images were acquired using a JEM-2100F TEM (JEOL, Japan) to characterize the dispersion, particle size and lattice spacing of the samples. XRD spectra were recorded using a D8 Advance diffractometer (Bruker, Germany, $K\alpha = 1.5406$ A) to characterize the lattice structure. FT-IR spectra were recorded on a FT-IR spectrometer (Nicolet 6700, Thermo Electron Co., USA) to characterize the composition and structure of the samples. The XPS spectra of the samples were recorded using a Thermo Fisher Scientific ESCALAB 250Xi spectrometer (USA) to characterize the elemental composition of the samples. The fluorescence and absorption spectra of the samples were measured at room temperature using a time-resolved fluorescence spectrometer (FL3-22, Jobin-Yvon, USA) and a UV-visible spectrophotometer (UV2600, Shimadzu Corp., Tokyo, Japan), respectively, to characterize the optical properties. The temperature dependence of phosphorescence was characterized by the Edinburgh FLS1000 device.

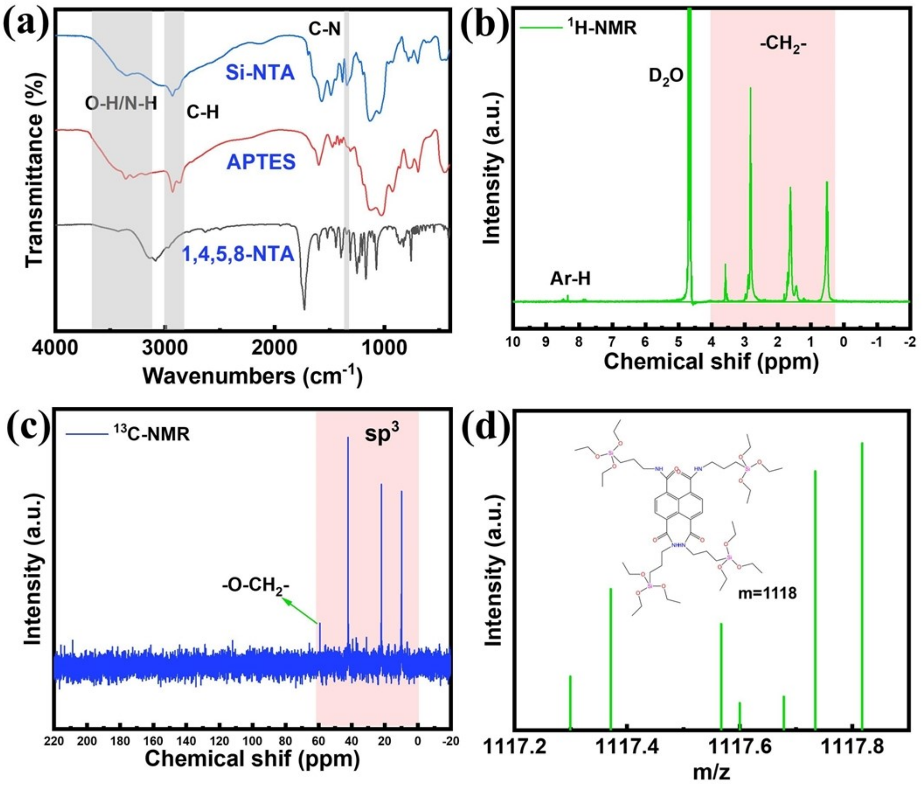

Figure S1. (a) The FT-IR spectra of the 1,4,5,8-NTA, APTES, and Si-NTA. (b)^{1}H-NMR of Si-NTA. (c) ^{13}C-NMR spectra of Si-NTA. (d) HR-MS spectra of Si-NTA.

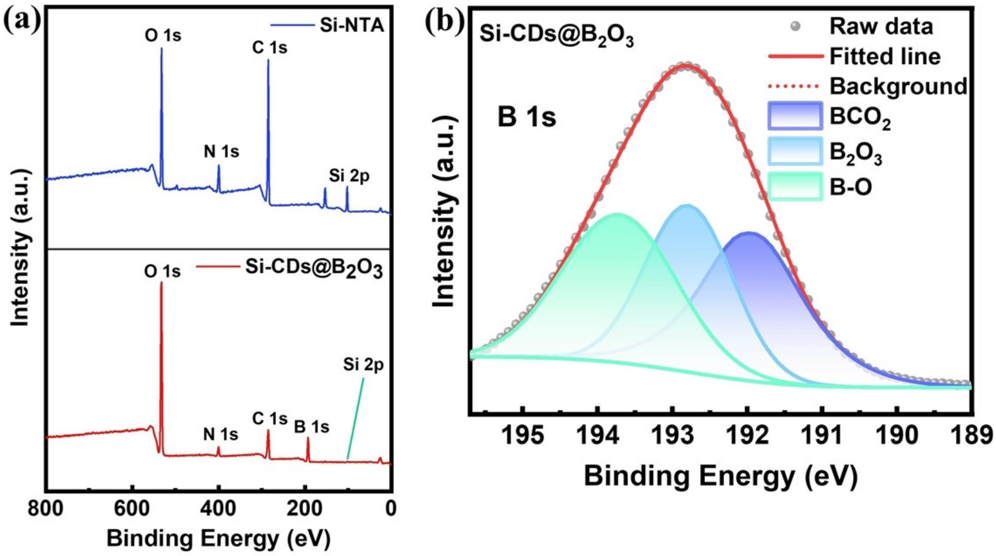

Figure S2. (a) Full XPS spectra of Si-NTA and Si-CDs@B_2O_3. (b) High-resolution B 1s spectra of Si-CDs@B_2O_3.

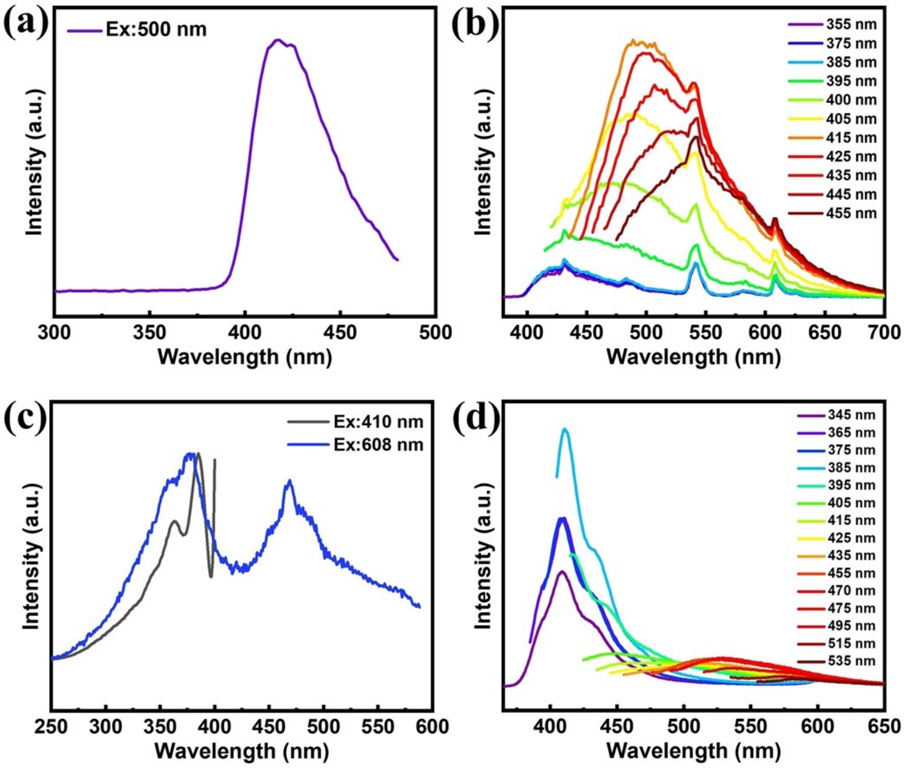

Figure S3. (a) Excitation spectra and (b) PL emission spectra of Si-NTA under different excitation wavelengths. (c) Excitation spectra and (d) PL emission spectra of Si-CDs@B_2O_3 under different excitation wavelengths.

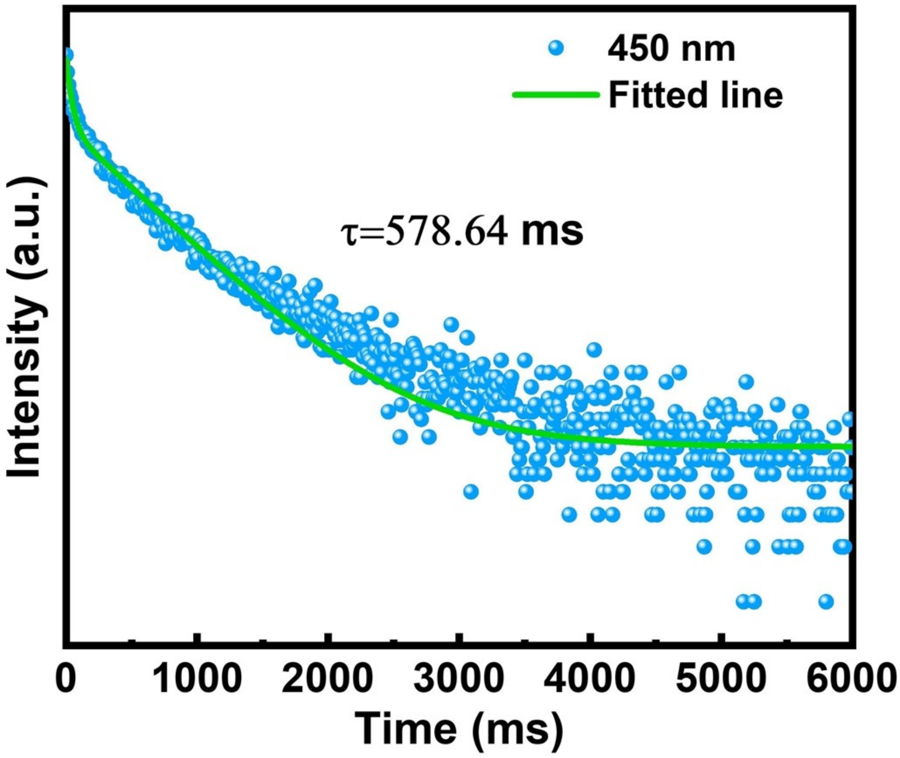

Figure S4. Time-resolved decay spectra of Si-CDs@B_2O_3 at room temperature with λ_{ex} = 310 nm.

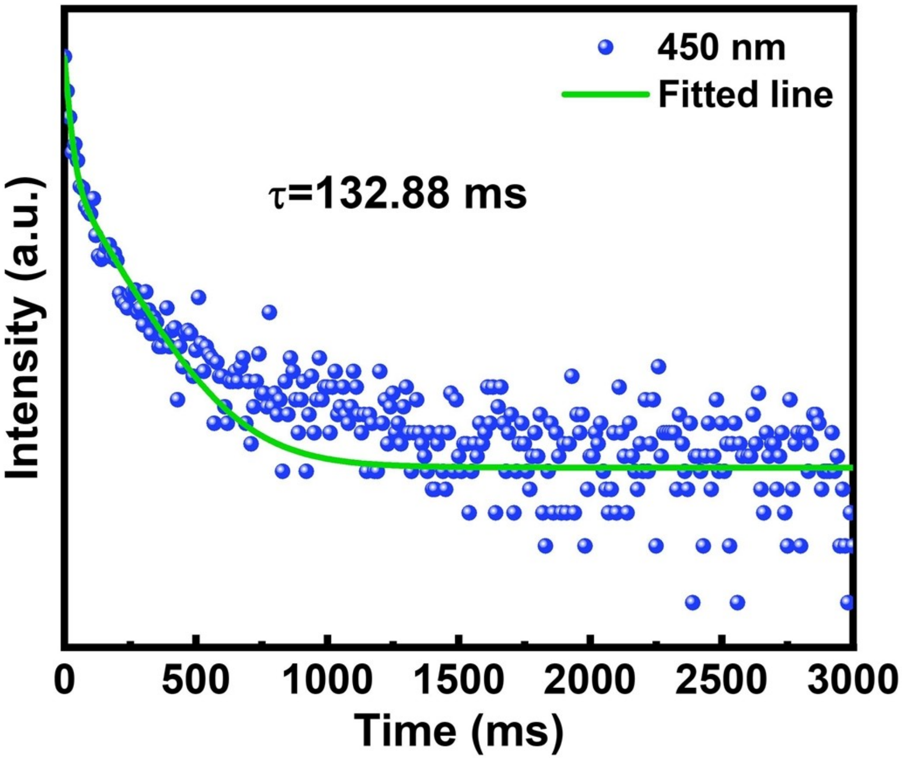

Figure S5. Time-resolved decay spectra of Si-CDs@B_2O_3 at room temperature with λ_{ex} = 365 nm.

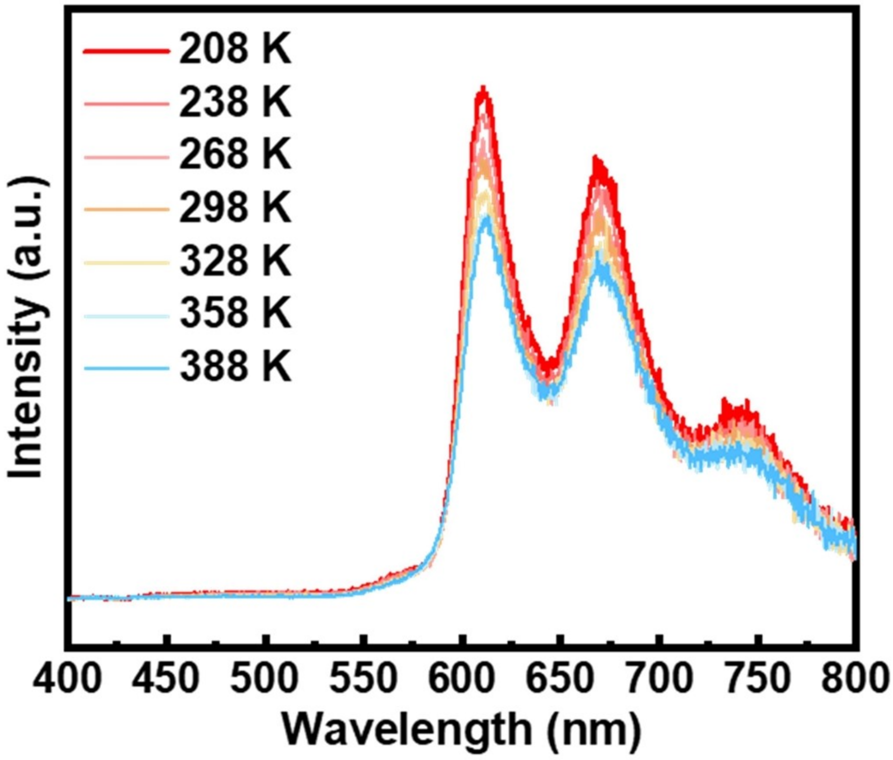

Figure S6. Phosphorescence emission spectra of Si-CDs@B_2O_3 at different temperatures with 1 ms delay.

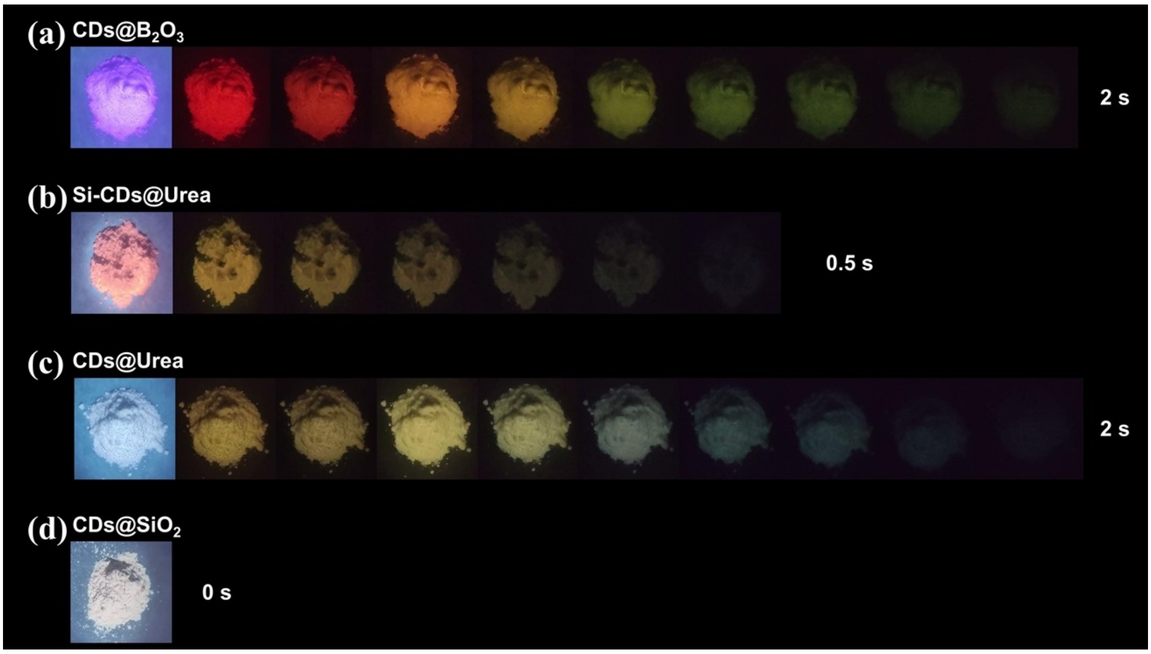

Figure S7. Optical images of comparison samples. (a) CDs@B_2O_3, (b) Si-CDs@Urea, (c) CDs@Urea, (d) CDs@SiO_2.

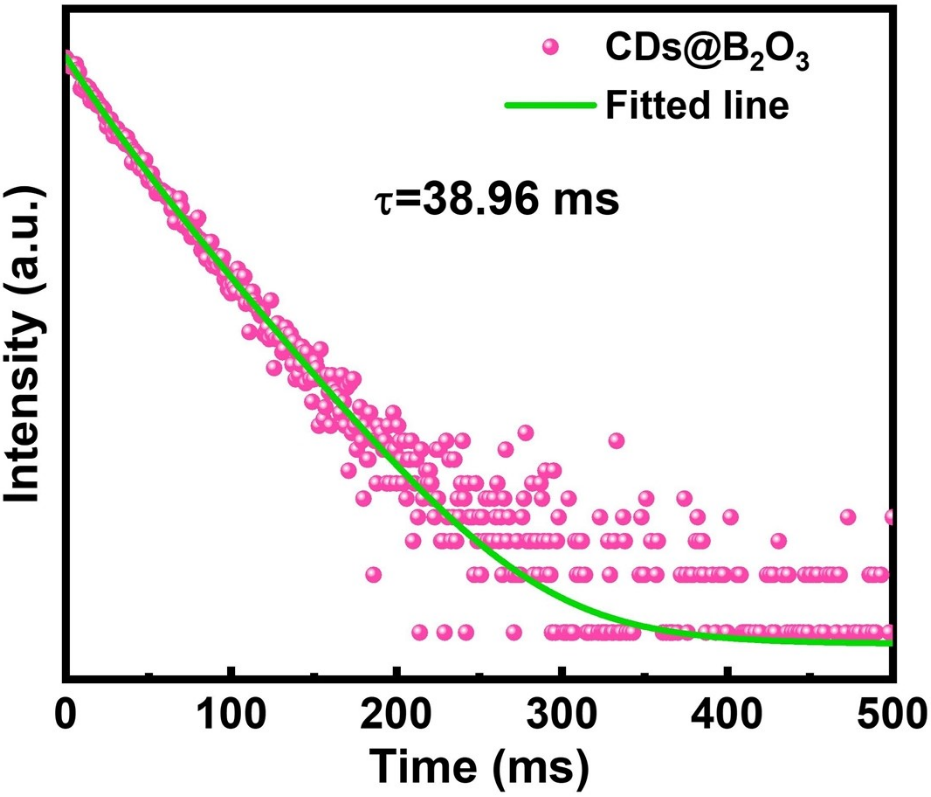

Figure S8. Time-resolved decay spectra of CDs@B_2O_3 at room temperature with λ_{ex} = 365 nm.

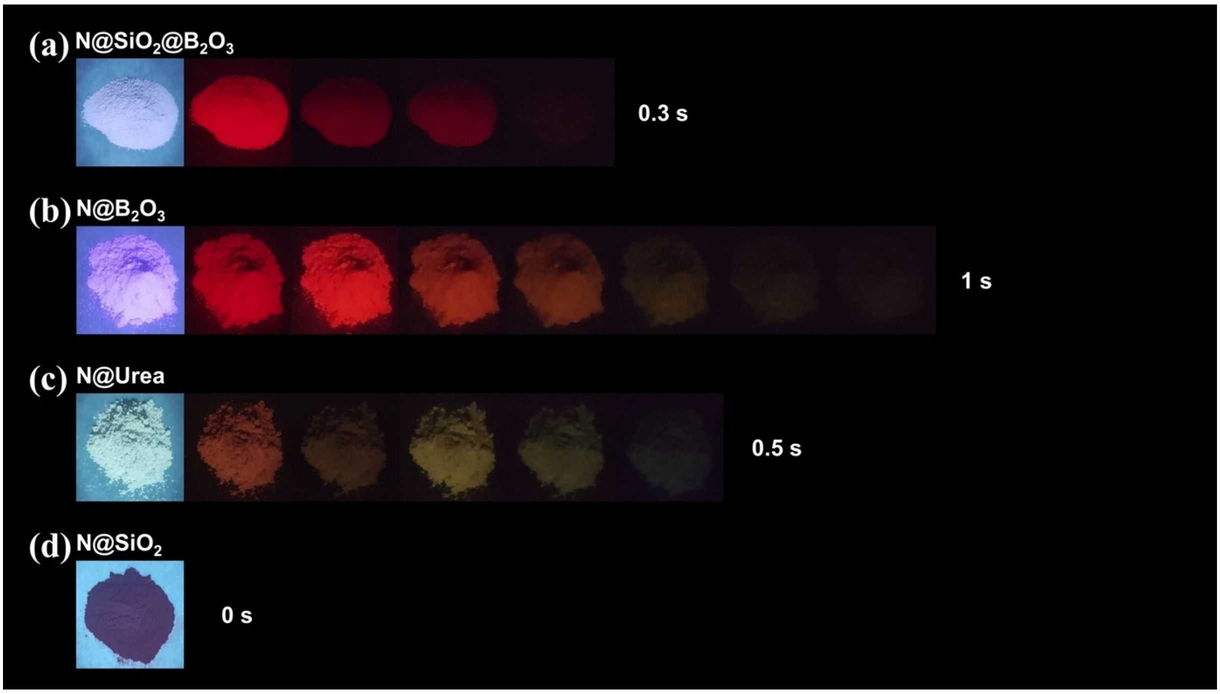

Figure S9. Optical images of comparison samples. (a) $N@SiO_2@B_2O_3$, (b) $N@B_2O_3$, (c) N@Urea, (d) $N@SiO_2$.

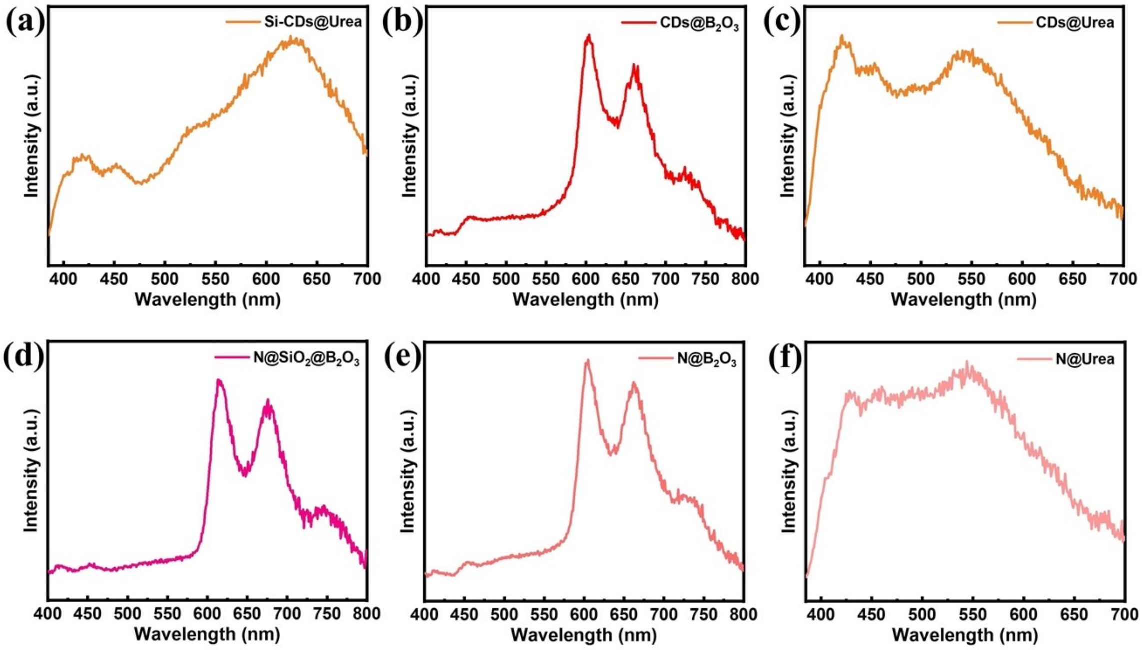

Figure S10. Phosphorescence spectra of comparison samples. (a) Si-CDs@Urea, (b) $CDs@B_2O_3$, (c) CDs@Urea, (d) $N@SiO_2@B_2O_3$, (e) $N@B_2O_3$, (f) N@Urea.

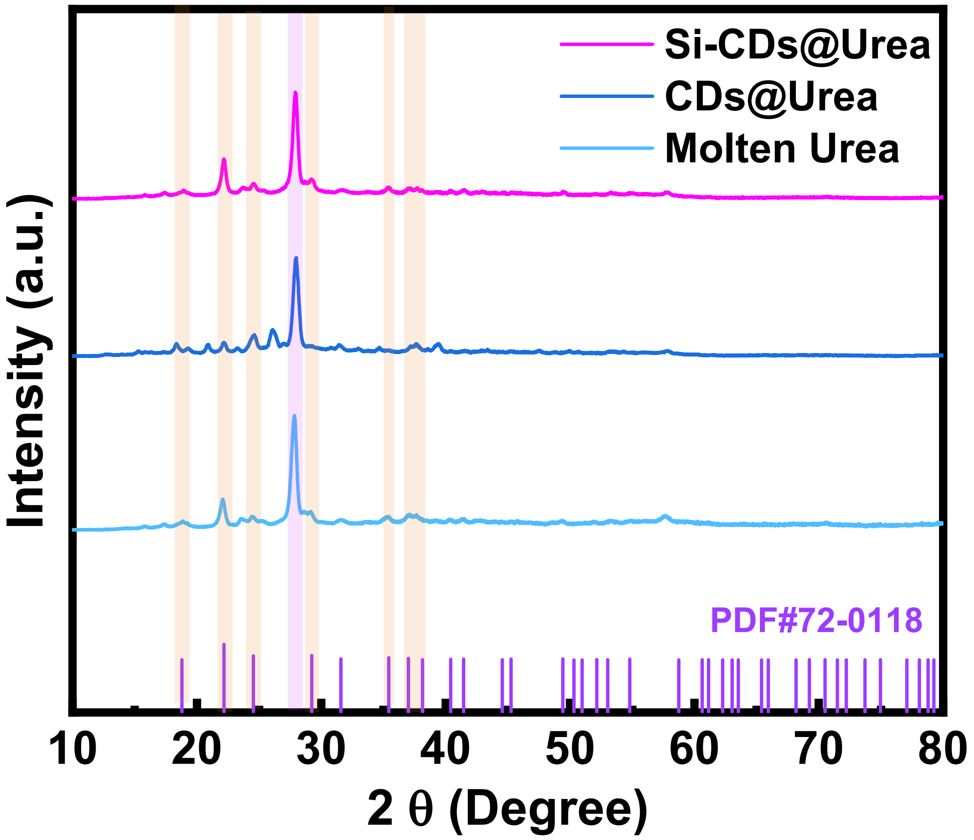

Figure S11. The XRD spectra of Si-CDs@Urea, CDs@Urea, and Molten Urea.

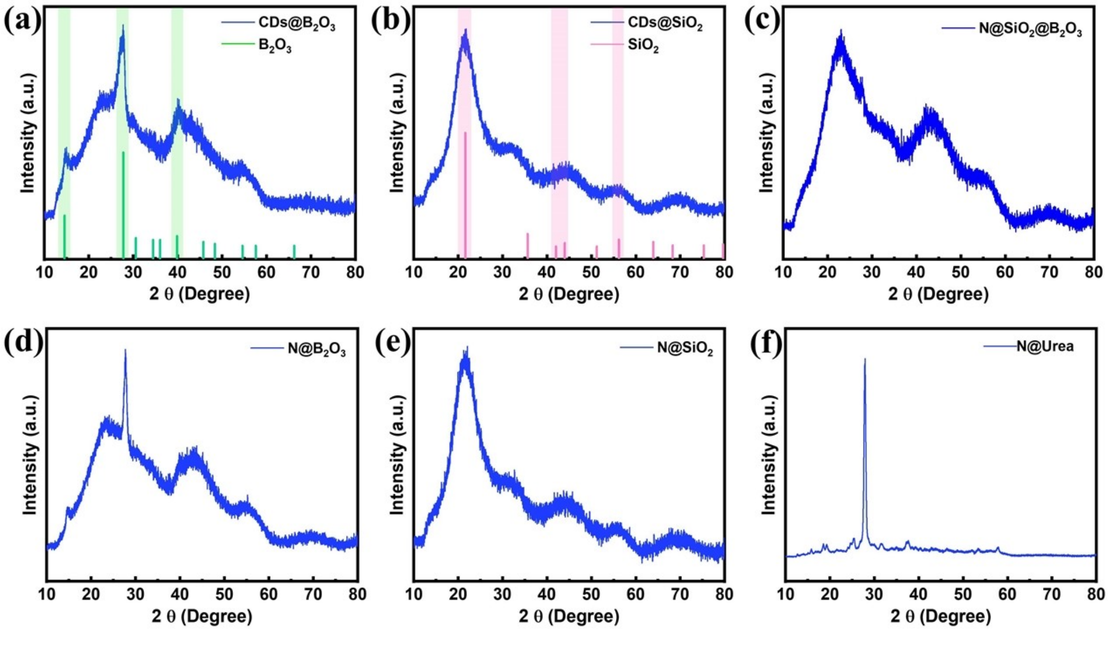

Figure S12. The XRD spectra of comparison samples. (a) CDs@B_2O_3, (b) CDs@SiO_2, (c) N@SiO_2@B_2O_3, (d) N@B_2O_3, (e) N@SiO_2, (f) N@Urea.

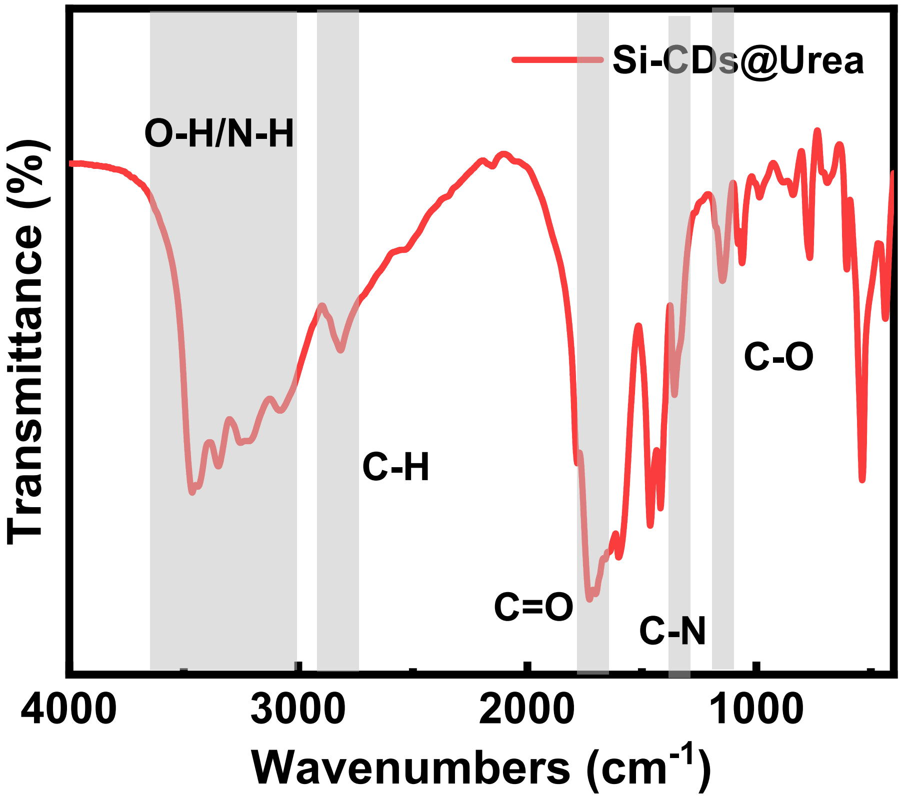

Figure S13. The FT-IR spectra of Si-CDs@Urea.

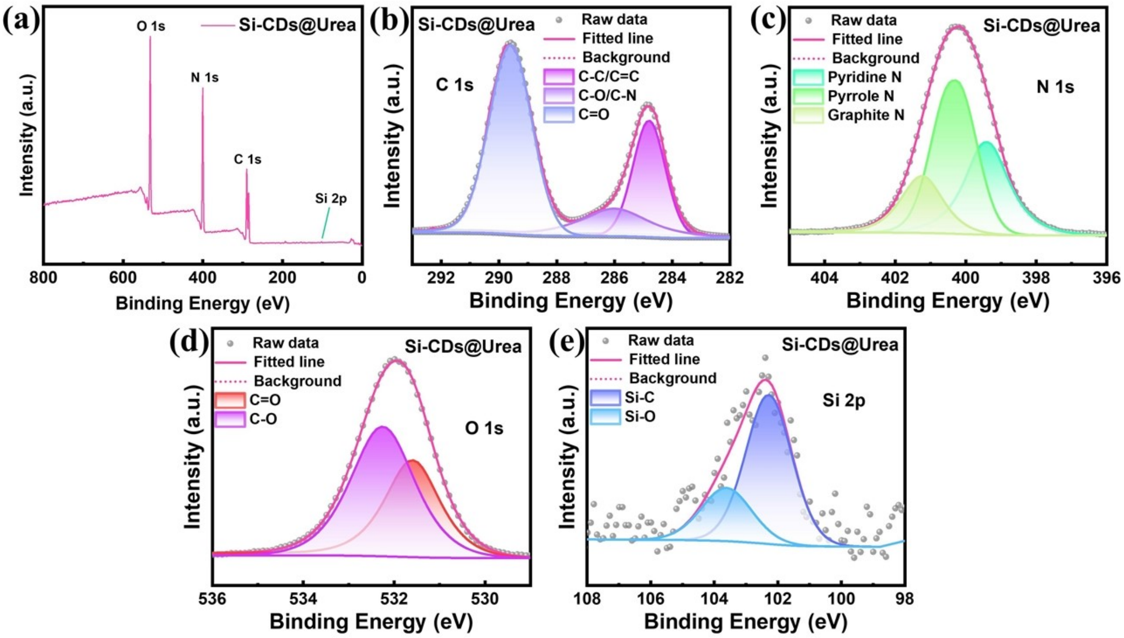

Figure S14. (a) Full XPS spectra of Si-CDs@Urea. (b-e) High-resolution C 1s, N 1s, O 1s and Si 2p spectra of Si-CDs@Urea. (b) C 1s, (c) N 1s, (d) O 1s, (e) Si 2p.

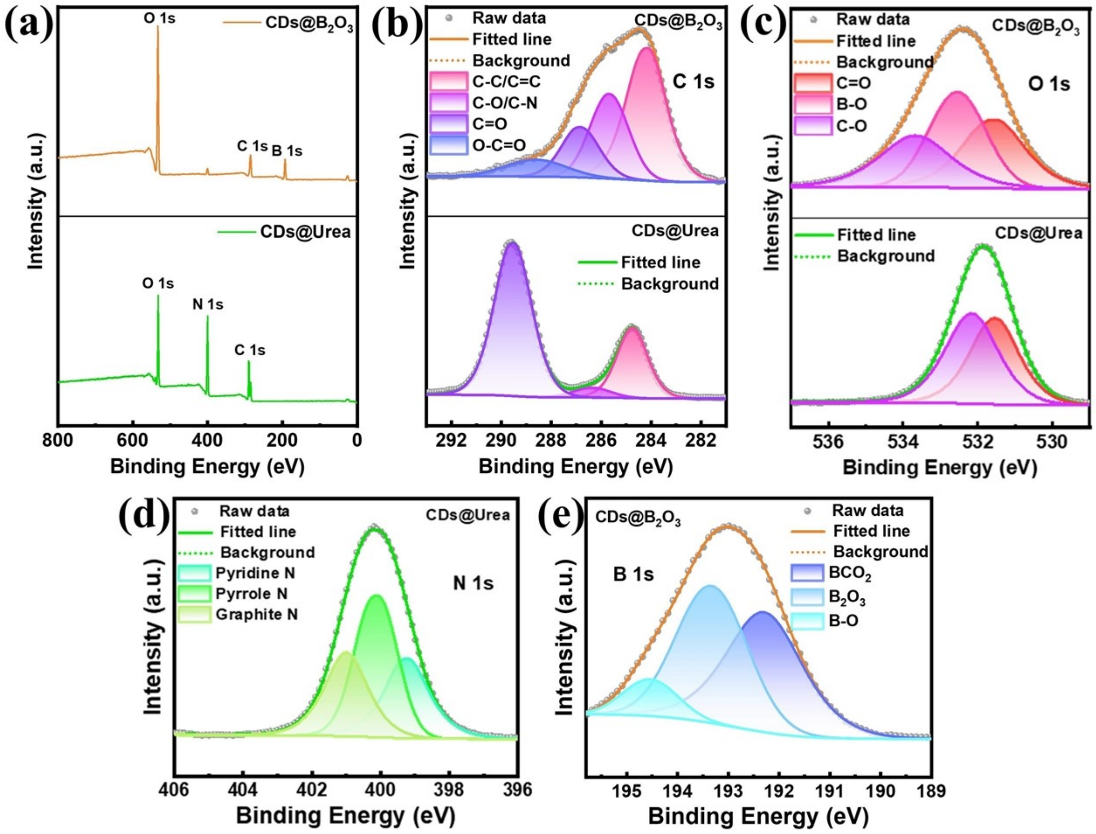

Figure S15. (a) Full XPS spectra of CDs@B_2O_3 and CDs@Urea. (b) High-resolution C 1s spectra of CDs@B_2O_3 and CDs@Urea. (c) High-resolution O 1s spectra of CDs@B_2O_3 and CDs@Urea. (d) High-resolution N 1s spectra of CDs@Urea. (e) High-resolution B 1s spectra of CDs@B_2O_3.

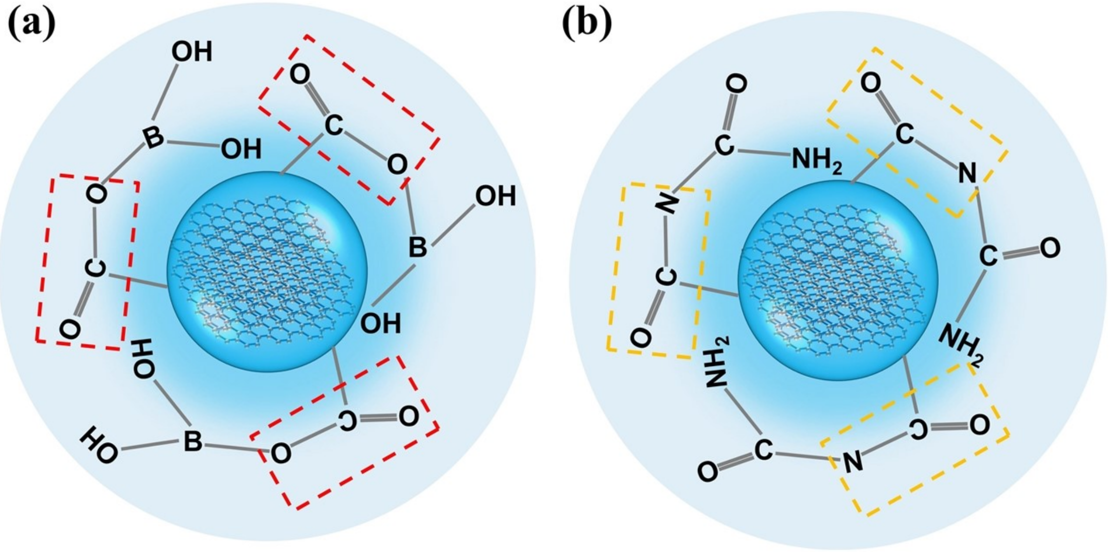

Figure S16. Possible bonding modes between CDs and different matrixes. (a) BA, (b) Urea.

Table S1. Summary of different synthetic strategies and phosphoresce emission properties of TDPC CDs.

Year	Method	Matrix	PER	PC	Lifetime	App.	Ref.
2021	Heating treatment+Calcination	B_2O_3	500-440 nm	Green → Blue	1.89 s 2.15 s	Information encryption Fingerprint detection	1
2021	One-step melting treatment	BA	478-606 nm	Orange → Yellow → White → Cyan	0.576 s 0.609 s 1.597 s	Anti-counterfeiting	2
2023	Solvothermal+ Oil bath	Urea+SiO_2 +NaOH	640-535 nm	Orange → Green	77.8 ms 109.6 ms 119.7 ms	Anti-counterfeiting	3
2023	Hydrothermal	NaCl+$MgCl_2$	560-528 nm	Yellow → Green	464 ms	Information encryption	4
2023	Pyrolysis	Al_2O_3	400-500 nm	Blue → Green	96 ms 911 ms	Information encryption	5
2023	Hydrothermal	PAA	645-550 nm	Orange → Green	142 ms 205 ms	Information encryption	6
2023	Hydrothermal+ Calcination	SiO_2	580-500 ms	Yellow → Green	0.9 s 1.28 s	Information encryption	7
2023	Heating treatment	BA	579-515 ms	Yellow → Green	0.94 ms 1.50 ms	Anti-counterfeit and Information encryption	8
2023	Hydrothermal	SiO_2	425-505 nm	Blue → Green	425.6 ms 1506 ms	Anti-counterfeit and Information encryption	9
2024	Pyrolysis	Urea	725-550 nm	Red → Yellow→ Green	56.69 ms 238.19 ms	Information Encryption	10
2024	Hydrothermal	RHO	430-505 nm	Deep blue → Green	238.7 ms 823.8 ms	Information encryption	11
2025	**Hydrothermal + Calcination**	**SiO_2+B_2O_3**	**743-450 nm**	**Red → Orange→ Yellow → Green → Cyan blue**	**48.53 ms 132.88 ms**	**Anti-counterfeit and Information encryption**	**This work**

PER: Phosphorescent emission range. PCs: Phosphorescent colors. Lifetime: Phosphorescence lifetime. App.: Applications

References:

1 Z. Zhou, Z. Song, J. Liu, B. Lei, J. Zhuang, X. Zhang, Y. Liu and C. Hu, Energy Transfer Mediated Enhancement of Room-Temperature Phosphorescence of Carbon Dots Embedded in Matrixes, *Adv. Opt. Mater.*, 2021, **10**, 2100704.

2 S. Cui, B. Wang, Y. Zan, Z. Shen, S. Liu, W. Fang, X. Yan, Y. Li and L. Chen, Colorful, time-dependent carbon dot-based afterglow with ultralong lifetime, *Chem. Eng. J.*, 2021, **431**, 133373.

3 Q. Lou, N. Chen, J. Zhu, K. Liu, C. Li, Y. Zhu, W. Xu, X. Chen, Z. Song, C. Liang, C.-X. Shan and J. Hu, Thermally Enhanced and Long Lifetime Red TADF Carbon Dots via Multi-Confinement and Phosphorescence Assisted Energy Transfer, *Adv. Mater.*, 2023, **35**, 2211858.

4 W. Shi, R. Wang, J. Liu, F. Peng, R. Tian and C. Lu, Time-dependent Phosphorescence Color of Carbon Dots in Binary Salt Matrices through Activations by Structural Confinement and Defects for Dynamic Information Encryption, *Angew. Chem. Int. Ed.*, 2023, **135**, e202303063.

5 L. Zhang, X. Chen and Y. Hu, Pyrolysis of Al-Based Metal-Organic Frameworks to Carbon Dot-Porous Al_2O_3 Composites With Time-Dependent Phosphorescence Colors for Advanced Information Encryption, *Small*, 2023, **20**, 2305185.

6 C. Kang, S. Tao, F. Yang, C. Zheng, Z. Qu and B. Yang, Enabling Carbonized Polymer Dots with Color-tunable Time-dependent Room Temperature Phosphorescence through Confining Carboxyl Dimer Association, *Angew. Chem. Int. Ed.*, 2023, **136**, e202316527.

7 J. Chen, J. Tan, P. Liang, C. Wu, Z. Hou, K. Shen, B. Lei, C. Hu, X. Zhang, J. Zhuang, L. Sun, Y. Liu and M. Zheng, Dynamic Room Temperature Phosphorescence of Silane-Functionalized Carbon Dots Confining within Silica for Anti-Counterfeiting Applications, *Small*, 2023, **20**, 2306323.

8 Y. Chang, N. Fu, M. Chen, Y. Zhang, F. Li, Z. Liu, F. Wang, G. Yue, X. Li and L. Guan, Achieving tunable time-dependent delayed emission color via dynamic competition between the matrix and carbon dots for anti-counterfeiting and multidimensional encryption, *Chem. Eng. J.*, 2023, **479**, 147808.

9 M. Shi, Q. Gao, J. Rao, Z. Lv, M. Chen, G. Chen, J. Bian, J. Ren, B. Lü and F. Peng, Confinement-Modulated Clusterization-Triggered Time-Dependent Phosphorescence Color from Xylan-Carbonized Polymer Dots, *J. Am. Chem. Soc.*, 2023, **146**, 1294-1304.

10 J. Sun, Z. Sun, Z. Wang, N. Wang, Y. Han, L. Zhang, B. Zhang and X. Zhang, Ultra-Long-Lived Red TADF-CDs: Solid-State Synthesis, Time-Dependent Phosphorescence Color And Luminescent Mechanism, *Adv. Opt. Mater.*, 2024, **12**, 2302542.

11 S. Zong, J. Zhang, X. Yin, J. Li and S. Qu, Time-Dependent and Excitation-Dependent Afterglow Color Evolution from the Assembly of Dual Carbon Dots in Zeolite, *Nano Lett.*, 2024, **24**, 1859-1866.